AAS 10-128

INVESTIGATION OF ALTERNATIVE RETURN STRATEGIES FOR ORION TRANS-EARTH INJECTION DESIGN OPTIONS

Belinda G. Marchand[*], Sara K. Scarritt[†], Thomas A. Pavlak[‡] Kathleen C. Howell[§], and Michael W. Weeks[¶]

The identification of feasible return trajectories that target, from the Moon, a precise location and approach vector at Earth entry is sensitive to the quality of the startup arc provided and the associated maneuver planning. These sensitivities are especially evident in the trans-Earth injection phase for Orion. As envisioned, a return from a lunar polar orbit employs three deterministic maneuvers. The concept behind this return strategy is rooted in conic analysis. The present study considers precision entry targeting from the perspective of the multi-body problem. A dynamical systems approach considers the intersection of entry interface dispersion manifolds with the Hill sphere of the Earth-Moon system. The locus of the intersections serves as a guide during the design of the departure sequence and offers a good measure of the likelihood of success in precision entry targeting based on that arc.

INTRODUCTION

Precision targeting, in this study, refers to the identification of all maneuvers necessary to guide the vehicle to a specific location on the rotating Earth with a pre-specified approach vector at entry interface. In the perturbed Earth-Moon system, this process is highly sensitive to the quality of the startup solution. It is also sensitive to the maneuvers associated with the startup arc. These sensitivities are evident in the trans-Earth injection phase of Orion. The startup arcs employed, in this case, often rely on conic approximations and notions. For instance, a three-maneuver sequence is commonly envisioned as the nominal case for the trans-Earth phase. The first trans-Earth injection (TEI) maneuver is designed to raise apoapsis of the initial lunar orbit. The second maneuver accomplishes the necessary inclination change. Finally, the third maneuver injects the spacecraft into its final return path. The sequence and the associated maneuver schedule are illustrated in Figures 1(a)-1(b).

Of course, two-body approximations[1] are not necessarily accurate for trajectory design in multi-body regimes. This is particularly true when the path of the vehicle is expected to escape the Hill sphere with a relatively low energy level. As the vehicle transitions through this dynamically sensitive region, the gravitational influence of the primaries and the perturbing bodies can introduce significant deviations from the intended path. This, in turn, affects the efficiency of algorithms that seek to fine tune the departure parameters to achieve precision entry at Earth. It also affects the subset of phase space explored by the algorithms in attempting to identify a feasible transfer.

[*] Assistant Professor, The University of Texas at Austin, 210 E. 24th St., Austin, TX 78712.
[†] Graduate Student, The University of Texas at Austin, 210 E. 24th St., Austin, TX 78712.
[‡] Graduate Student, Purdue University, 701 W. Stadium Ave., West Lafayette, IN 47907.
[§] Hsu Lo Professor, Purdue University, 701 W. Stadium Ave., West Lafayette, IN 47907.
[¶] GNC Engineer, NASA JSC, 2101 NASA Pkwy. Houston, Texas 77058 / EG-6.

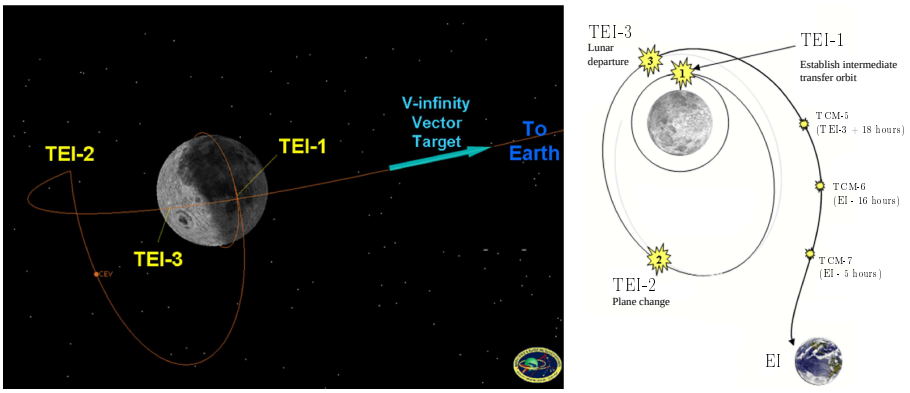

(a) Return Trajectory (b) Maneuver Schedule

Figure 1. Orion Trans-Earth Trajectory and Maneuver Schedule

The investigation is focused, first, on developing a better understanding of the sensitivities associated with a precision entry at Earth. This is accomplished by propagating a representative sample of dispersion trajectories for each of the six possible Earth Entry Interface (EEI) states considered for Orion. The EEI state parameters are associated by an altitude of 121.912313 km, and an entry speed of 10.992728 km/s. Then, each EEI state is uniquely determined by their geocentric latitude and longitude, the flight path angle, and flight path azimuth as defined in Table 1.

Table 1. Entry Interface Parameters

Entry Parameter	EEI-1	EEI-2	EEI-3	EEI-4	EEI-5	EEI-6
Longitude	-115.5°	-121.00°	-134.5456°	-151.4038°	173.5216°	175.6365°
Latitude	-46.66992°	-8.8522°	-19.20410°	-7.14720°	15.36700°	15.36700°
Flight Path Azimuth	0.0°	0.0°	13.9960°	34.1065°	62.3311°	49.3291°
Flight Path Angle	-5.81°	-5.99°	-6.03°	-6.16°	-6.16°	-5.86°

Together, the resulting set of dispersion trajectories are treated as a segment of a "manifold" surface associated with a particular EEI state. That is, this surface represents the subset of the dynamical flow that converges onto the vicinity of the specified entry state in forward time.

The intersection of the dispersion manifolds with the Hill sphere is useful in more accurately designing improved startup solutions. The Hill sphere is defined in the synodic rotating frame of the Earth-Moon circular restricted three-body problem (CR3BP).[2,3] In this frame, it is assumed that the primaries (i.e. the Earth and Moon) evolve along circular orbits about their common center of mass. The rotating x-axis is directed from the Earth to the Moon such that both primaries remain equidistant along that line for all time. The z-axis is normal to the plane of their orbits while the y-axis completes the right-handed triad. The Hill sphere itself is centered at the smaller of the two primary bodies, in this case the Moon. The radius of the sphere is approximately determined as

$$r_s = a\sqrt[3]{\frac{\mu_{Moon}}{3\mu_{Earth}}}. \tag{1}$$

The relative size of the Hill sphere, in relation to the Earth, Moon, and the libration points of the Earth-Moon CR3BP is illustrated in Figure 2.

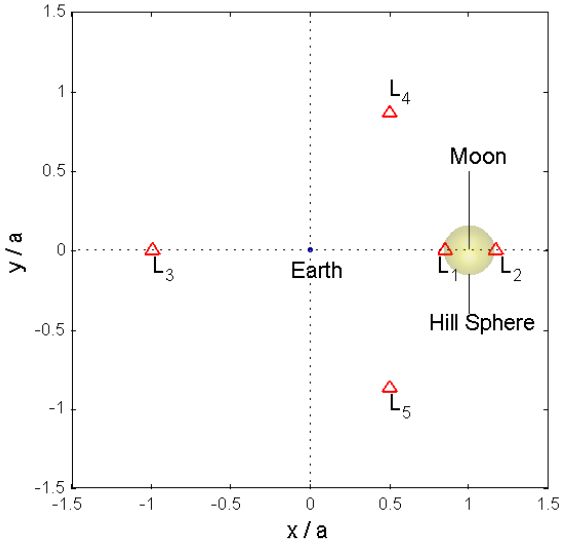

Figure 2. CR3BP Hill Sphere: Earth Centered Synodic Frame

The intersection of each dispersion manifold with the Hill sphere can be represented as a locus of points. The collection of all dispersion loci for a given EEI state are useful, for instance, in identifying whether a departure strategy for one EEI state is also suitable for one or any of the remaining five. The loci are also useful in designing alternate departure schemes, specifically those that consider the use of non-conic arcs derived from multi-body analysis. The understanding gained from the study of the dispersion loci allows the designer to determine whether or not a conic departure strategy is likely to succeed, how it could be modified, or whether an alternate departure strategy is necessary. Furthermore, at the very least, designing startup arcs in the synodic frame is useful by the simple fact that the Earth and Moon are both fixed on this frame. Thus, at least one can identify startup arcs that lead to the general vicinity of the Earth. The improved quality of the startup arcs would lead to a more computationally effective targeting process.

In either targeting[4–6] or optimization,[7,8] the startup arc affects more than just the computational effort. It also determines the neighborhood of phase space that is explored by the algorithm. Both targeting[4–6] and trajectory optimization[9–12] algorithms explore only the immediate vicinity of the reference solution. As a result, the solutions identified often resemble the startup arc in many ways. This excludes, however, many other types of solutions that may offer improved trajectory options. Thus, developing a better understanding of the dynamical flow associated with the types of solutions sought is an important initial step in any targeting or optimization process.

A dynamical systems approach has often proven essential in acquiring this understanding in multi-body regimes.[13–15] The process characterizes the phase space into stable, unstable, and center manifold flows around a reference solution. The present study is an initial step in that direction. The general intent is to understand and exploit the dynamical structure of the Earth-Moon system to identify feasible and lower cost startup arcs that more closely satisfy the mission criteria a priori. No restrictions are placed on the geometry of the solutions or the location of the maneuvers.

The analysis presented here is initially focused on the dispersion analysis. The precision entry

problem, for Orion, targets at most five quantities: altitude, flight path angle, geocentric latitude and longitude, and flight path azimuth.[5] The altitude, latitude, and longitude determine the position components of the EEI state. The flight path angle and azimuth, then, characterize the approach vector for the incoming velocity. The entry speed itself is not constrained. However, for the purpose of constructing the dispersion manifolds, a representative entry speed is selected and held fixed. Then, one at a time, each of the remaining entry parameters is perturbed relative to their nominal values. These perturbed entry states are defined in the Earth Mean Equator and Equinox of J2000 frame. This is consistent with the reference frame employed in the JPL DE405 ephemeris.[16] That is, the inertial X-Y plane is defined as the Earth Mean Equator, the inertial X axis is aligned with the Vernal Equinox of J2000, the inertial Z axis is normal to the plane, and Y completes the triad. Subsequently, these inertial perturbed states are numerically integrated backwards in time in the ephemeris model. The ephemeris model, in this case, assumes the Sun, Earth, and Moon states are available directly from the DE 405 ephemeris.[16] Thus, only the spacecraft state is numerically integrated while the states of the primaries and perturbing bodies are assumed to be known functions of time. The trajectories associated with one of the five entry parameters are used to construct the dispersion manifold for that quantity.

For each EEI state, then, a total of five dispersion manifolds are generated. The associated trajectories are transformed into the synodic rotating frame of the Earth-Moon system,[17] where the mean Hill sphere is defined. The loci of intersections of the dispersion manifolds with the Hill sphere are identified. Then, the significance of the intersection loci, and their impact on lunar departure strategies, is addressed.

To illustrate the impact of third and fourth body effects on the return strategy, a series of examples are considered next. At first, the examples are focused on the emergency contingency case: targeting only altitude and flight path angle. A targeting algorithm[5] is applied on a reasonable yet infeasible solution so that the entry altitude and flightpath angle are met without violating the total cost constraints. However, as previously mentioned, the quality of that startup arc limits the neighborhood that targeting and non-evolutionary optimization algorithms explore. Thus, continuation schemes are applied on the resulting arcs to explore the available solution space further and lower the transfer costs. Significant cost reductions are achieved as a result. The newly converged solutions are employed in a targeting algorithm[5] to assess the sensitivity of the entry parameters relative to the startup solution.

Dispersion Analysis

Earlier studies obtain startup arcs for the three maneuver return sequence by dividing the design process into two parts.[1] First, the a lunar return segment is designed, in a Moon Centered Inertial (MCI) frame, using conic arcs. Specifically, the spacecraft in low lunar orbit performs a maneuver to raise apoapsis, then a second maneuver to change the inclination of the plane, and a third maneuver to raise the energy enough to escape the vicinity of the Moon in the general direction of the Earth. These maneuvers, planned in the two-body problem, are then implemented in the ephemeris model of the lunar segment. Of course, the resulting path – in the ephemeris model – does not resemble the two-body solution due to the impact of third body effects on this particular type of return sequence. The second part of the process is to take a partial state at Earth entry, make some assumptions about the remaining states, and propagate that backwards in time until the trajectory crosses a user specified interface region.[1] The results are then used in an optimal targeting process that seeks to bridge the gap at the interface region and also meet the remaining constraints along the path. One

drawback of this approach is that the startup arcs obtained from this two-body approximation can exhibit large spatial and temporal discontinuities at the interface region. This can have a negative impact on the numerical efficiency of any targeting or optimization algorithm that only explores the vicinity of the startup arc for feasible or optimal solutions. It is also true that even if the discontinuity is not unreasonable at the interface region, the entry state was not fully specified during the backward propagation of the Earth segment. Thus, either feasible or optimal targeting algorithms would have to both bridge the spatial and temporal gap at the interface region and potentially correct very large errors in the entry state.

Precision entry, in this case, requires that the vehicle achieve specific altitude, flight path angle, flight path azimuth, and geocentric latitude and longitude at Earth entry. Of these quantities, the geocentric longitude and the flight path azimuth are both measured in coordinate frames that are fixed on the rotating Earth. Thus, the entry time becomes a critical factor in determining whether or not the entry state is met.

The numerical determination of the dispersion manifolds for a specific entry interface state begins with the selection of a startup value for the entry speed, which is not itself constrained. Once specified, the full inertial state vector is available. The inertial entry state is subsequently integrated backwards in time through some stopping condition, typically based on radial distance or time of flight. This first arc defines the "nominal" path to the entry site specified. To generate the dispersion manifold, then, the "nominal" path, at the specified epoch time, is systematically perturbed. That is, errors are introduced in one of the five entry parameters: altitude, latitude, longitude, flight path angle, flight path azimuth. A corresponding Earth Centered Inertial (ECI) state is computed by assuming the entry speed to be 10.992728 km/sec. While holding the speed, the entry time, and all four remaining parameters fixed, the states associated with a specific set of perturbations are propagated backwards in time to generate the associated dispersion manifold. Once again, the integration process stops when a specific radial distance from the central planet or reference time of flight is exceeded.

Once the dispersion manifolds are generated, the next step is to determine whether or not the associated trajectories intersect the Hill sphere, selected here to define the lunar "interface" region. This is accomplished by transforming the dispersion manifolds into the Earth-Moon synodic frame and numerically searching for intersections with the Hill sphere. Naturally, whether or not intersections exist is largely dependent on timing. Specifically, the time associated with the Earth Entry Interface state. Initially, the entry time is adjusted manually, as needed, to guarantee the manifold intersects the Hill sphere. However, the process lends itself to the development of a timing condition for the Earth-Moon system.

To visualize the geometry of the intersections, the Hill sphere is divided into a standard grid of latitude and longitude. Here, longitude is measured along the Earth-Moon orbital plane, relative to the instantaneous Earth-Moon line. If the intersection occurs above the Earth-Moon plane, the latitude of the intersection along the sphere is defined as positive. Figures 3(a)-3(b) each illustrate five loci of points, which represent the intersections of a specific dispersion manifold with the sphere.

For each dispersion manifold, the range of perturbations that lead to trajectories that intersect the Hill sphere is summarized in Table 2. In relation to this data, the arrows listed in the legend for Figures 3(a)-3(f) indicate the direction of motion along the loci, from the minimum to the maximum values listed in Table 2. The direction of the flow along the loci is crucial to our understanding of constraint coupling, discussed later in this document.

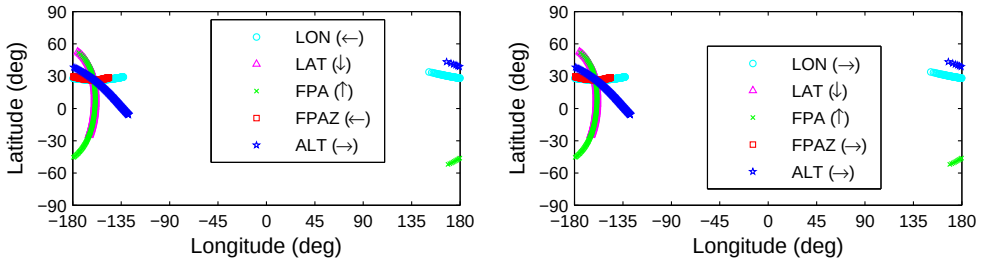

(a) EEI-1

(b) EEI-2

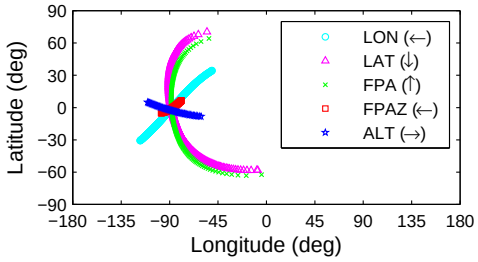

(c) EEI-3

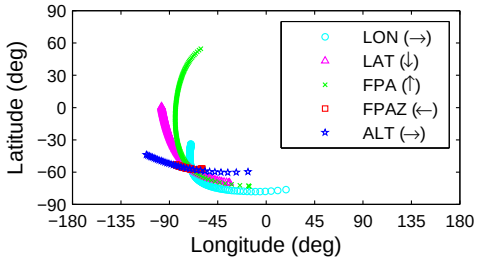

(d) EEI-4

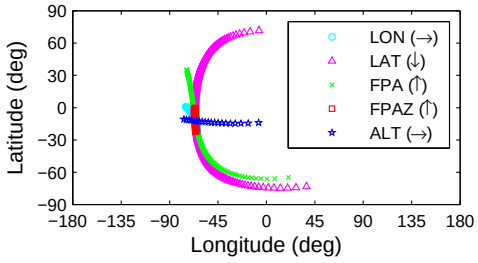

(e) EEI-5

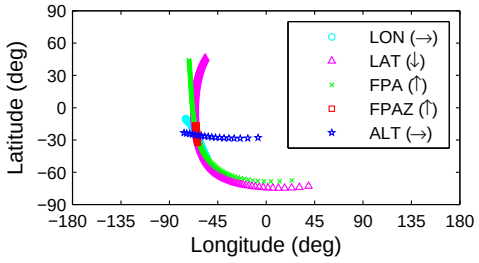

(f) EEI-6

Figure 3. Intersections of EEI Dispersion Manifolds with Hill Sphere

The Latitude and Flight Path Angle loci in Figures 3(a)-3(f) exhibit the largest spread along the hill sphere. However, of the angular quantities targeted, the data in Table 2 suggests that the flight path angle dispersion manifolds exhibit the least number of intersections with the Hill sphere. Thus, while the dispersion curve on the sphere appears wide, it is associated with a much smaller range of errors relative to the desired nominal value. This suggests small changes in flight path angle at entry have a significant effect on the overall geometry of the transfer arc near the Moon. Furthermore, although the altitude dispersion spread on the sphere does not appear as significant as flight path angle, many of the altitudes selected did not lead to intersections with the sphere. Of course, since the entry speed was fixed, this is not surprising since the only parameter targeted that affects orbital energy is the altitude at entry.

Table 2. EEI Range of Dispersion Errors That Lead to Intersections with Hill Sphere

EEI	Altitude (km)		Latitude (deg)		Longitude (deg)		Flight Path Angle (deg)		Flight Path Azimuth (deg)	
	Min.	Max.	Min.	Max.	Min.	Max.	Min.	Max.	Min.	Max.
1	-11.28	95.99	-2.93	10.00	-7.79	7.24	-7.34	1.43	-10.00	10.00
2	-1.25	4.76	-10.00	4.99	-3.63	10.00	-2.43	4.89	-10.00	10.00
3	-7.27	17.79	-8.85	9.95	-8.85	10.00	-4.69	3.73	-10.00	10.00
4	-30.83	4.76	-10.00	1.73	-6.29	4.34	-0.93	7.39	-10.00	10.00
5	-2.26	7.27	-9.95	8.05	-10.00	10.00	-5.69	5.34	-10.00	10.00
6	-2.26	6.27	-10.00	6.29	-10.00	10.00	-3.43	5.84	-10.00	10.00

Whether the dispersion manifolds intersect the Hill sphere, and how wide spread the dispersions are on the sphere itself, introduce two distinct issues that impact the design process. If, for instance, a two-body conic analysis is employed in selecting startup arcs, it is important that the dispersion manifolds for the desired EEI states intersect with the sphere in a favorable orientation. A startup arc with large state and/or temporal discontinuities at the interface region can have a detrimental effect on the computational efficiency of any targeting process. Large discontinuities at the interface state can also influence the subset of phase space that a targeting or optimization algorithm searches. This, in turn, can have a negative effect on the cost of merging the Earth and Moon segments and transitioning them into a single feasible transfer trajectory.

Of course, a wide range of dispersions on the Hill sphere is not, in itself, an undesirable feature. In fact, a wide dispersion on the Hill sphere may be indicative of increased flexibility regarding the quality of the startup arc. For instance, a startup arc that exhibits significant errors in that entry parameter may still qualify as a reasonable initial guess because properly scheduled maneuvers can identify neighboring trajectories that both (a) originate from the Moon and (b) are closer to the desired EEI state. This is demonstrated in the last section of this paper with the longitude and latitude constraints.

The flight path azimuth dispersions, in contrast, intersect the hill sphere for all six EEI states considered. That is, the entry flight path azimuth may be off by up to $\pm$ 10°, and the associated entry manifolds will still intersect the Hill sphere near the same region. However, Figures 3(a)-3(f) indicate that these intersections occur in a very narrow and confined region of the sphere, unlike the latitude and flight path angle dispersions which span a significant spread along the sphere. Thus, designing a lunar transfer, for precision entry, essentially requires that the lunar segment target a very precise neighborhood of the Hill sphere. For instance, let N_a denote the subset of the dispersions on the Hill sphere that correspond to errors in azimuth and N_l the subset of the dispersions that correspond to errors in latitude. The neighborhood defined by N_a is smaller, in

this case, than that defined by N_l. In designing the lunar segment of the trajectory, one seeks a startup arcs that exists in the region defined by $N_a \cap N_l$. Of course, this neighborhood only exists if $N_a \subset N_l$. Thus, the design of the startup arc, for a precision entry problem, is not trivial. Certainly, two-body approximations may not be suitable under such circumstances unless extremely close attention is devoted to targeting the precise neighborhood required on the Hill sphere. If the startup arc intersects the Hill sphere, but $N_a \cap N_l = \emptyset$, a targeting process may exhibit a significant reduction in performance, or even difficulties converging on a solution.

One last notable observation is that the dispersions for EEI #1 are all generally centered around the -180° longitude line, as seen from Figure 3(a). This clearly indicates that all dispersion trajectories intersect the Hill sphere between the Earth and the Moon, closest to the L_1 Earth-Moon libration point region. In contrast, the remaining sites tend to intersect the hill sphere along the $-\hat{\boldsymbol{y}}$ face, on the L_5 side. In fact, for EEI-2, the dispersion manifolds at the specified entry time extend beyond L_5 before bending towards the moon and intersecting the Hill sphere. The dispersion manifolds for EEI-6 and EEI-5 come close to L_5 but do extend beyond it for the epoch times selected. This information can be employed, in future studies, in identifying alternate transfer arcs, based on multi-body analysis, that better exploit the dynamical structure of the Earth-Moon system to achieve the specified precision entry goals.

Startup Arcs and Converged Solutions

As previously mentioned, the nominal return trajectory from low lunar polar orbit is often constructed from conic solutions. In this case, targeting or optimization algorithms are usually required in constructing general baseline transfer trajectories in an n-body regime, for $n > 2$. A multiple-shooting algorithm,[18,19] for instance, is one available method that is easily and successfully applied when constructing baseline trajectories. An advantage of multiple-shooting is that it is not problem specific. The same solution process is applicable in either the CR3BP or in the ephemeris model. The CR3BP, of course, offers a simplified framework from which to search for transfer arcs that may be better suited to address the complexities of the precision entry problem. In the end, the results must be accurately transitioned and reacquired in the ephemeris model. The process of transitioning solutions between models is easily accomplished with multiple shooting methods.

The first step in transitioning a solution between these two systems is to identify the appropriate state transformation. In the ephemeris model, the spacecraft states are typically represented in either Earth Centered Inertial (ECI) or Moon Centered Inertial (MCI) coordinates. In the CR3BP, spacecraft states are traditionally expressed in terms of non-dimensional synodic rotating frame coordinates.[17] While the mathematical relation between the ephemeris inertial frame and the synodic rotating frame is easily identified using the available planetary ephemerides, there is one key difference that must be noted. That is, in the CR3BP, the Earth-Moon distance is constant, but that is not the case in the ephemeris model. Subsequently, whenever a solution is transitioned across these two models, it is reacquired using a multiple shooting method to guarantee the resulting states lead to a feasible trajectory.

For instance, consider a baseline 1.5 km/sec solution, such as that labeled EPHEM (Nominal) in Figure 4. This solution is based on the three-burn sequence previously described. Once transitioned and numerically reacquired in the CR3BP, the resulting arc and a multiple shooting algorithm may be employed in a continuation scheme to explore other neighboring solutions. A sample three-burn 1.0 km/sec solution, resulting from this approach, is identified both in the CR3BP and in the ephemeris models. These arcs are illustrated in Figure 5.

Since the second maneuver in this improved 1.0 km/sec solution is considerably smaller, further explorations consider a two-maneuver strategy. Eventually, a 0.96 km/sec two-burn solution is identified. The 0.96 km/sec two-burn solution obtained in the CR3BP (ΔV = 1.0 km/sec), and the corresponding trajectory transitioned into the ephemeris model (ΔV = 0.96 km/sec), are both depicted on Figure 6. In this case, the inclination change originally implemented through the second maneuver is now accomplished by third body effects at the expense of an increase in time of flight of up to two days.

Trajectory design in the context of the multi-body problem offers a more diverse solution space, lower energy transfers with correspondingly lower costs, and greater flexibility for global entry targeting. Since lower cost solutions are usually associated with low energy transfers, an increase in time of flight is to be expected. However, a hybrid design approach that incorporates low and medium energy segments can be beneficial in future studies when identifying solutions that exhibit the best of both arcs.

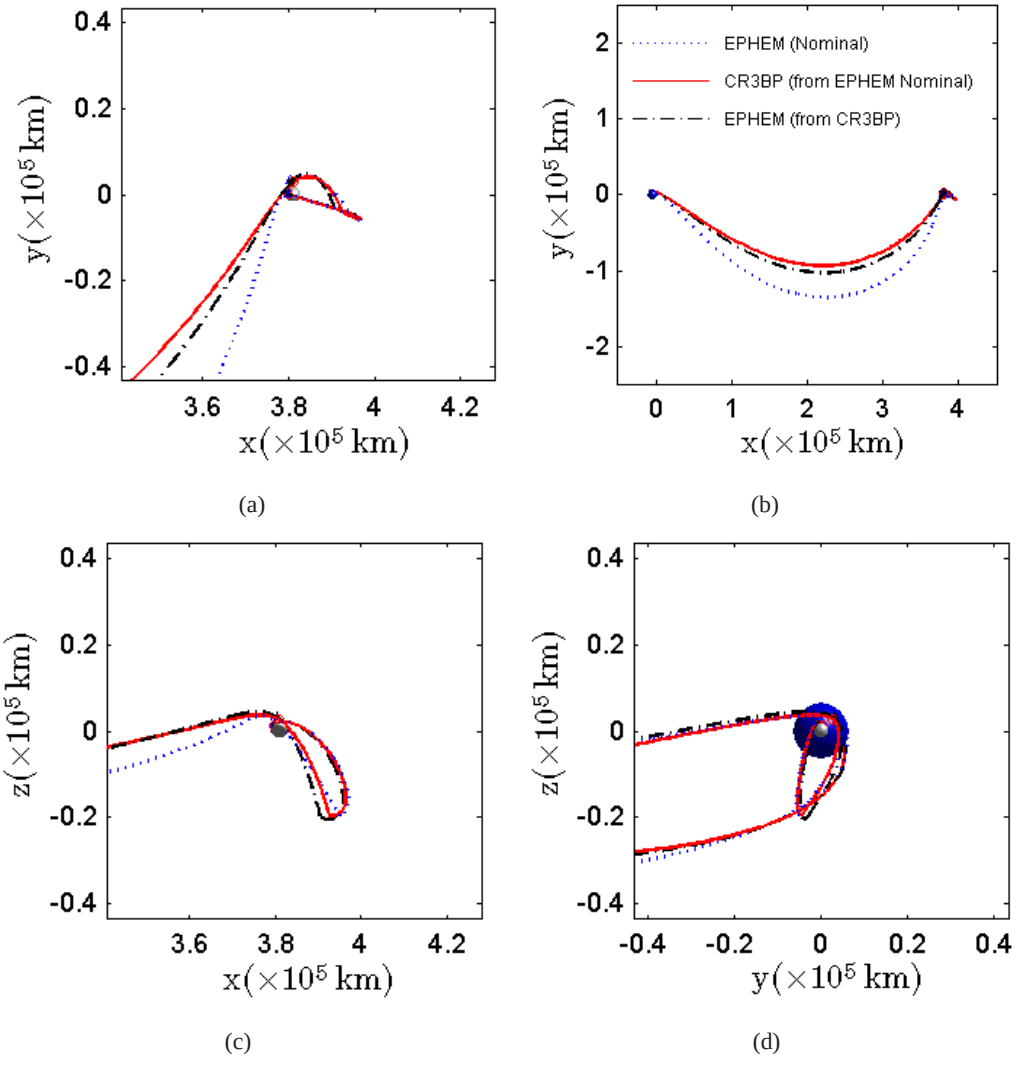

Figure 4. Three-Burn Solution: ΔV = 1.5 km/sec

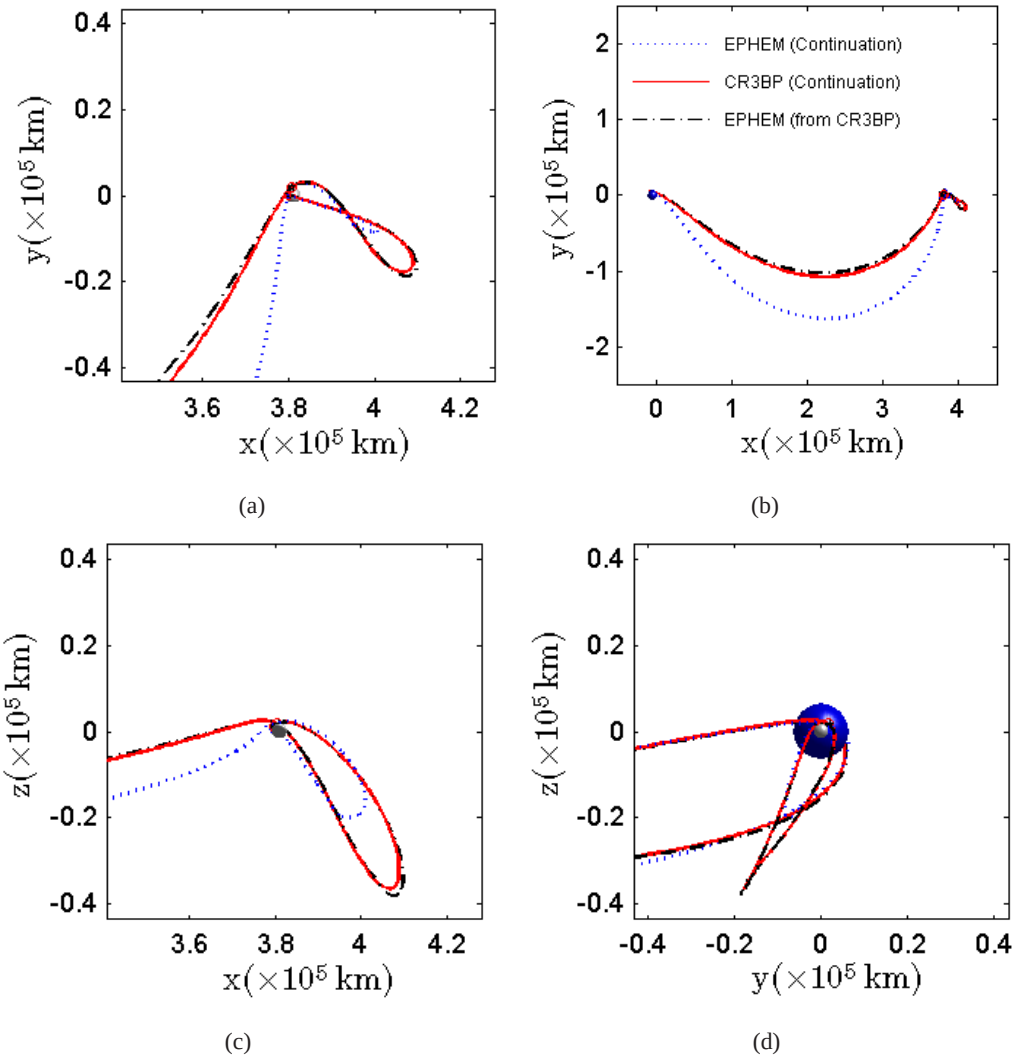

Figure 5. Three-Burn Solution: ΔV = 1 km/sec

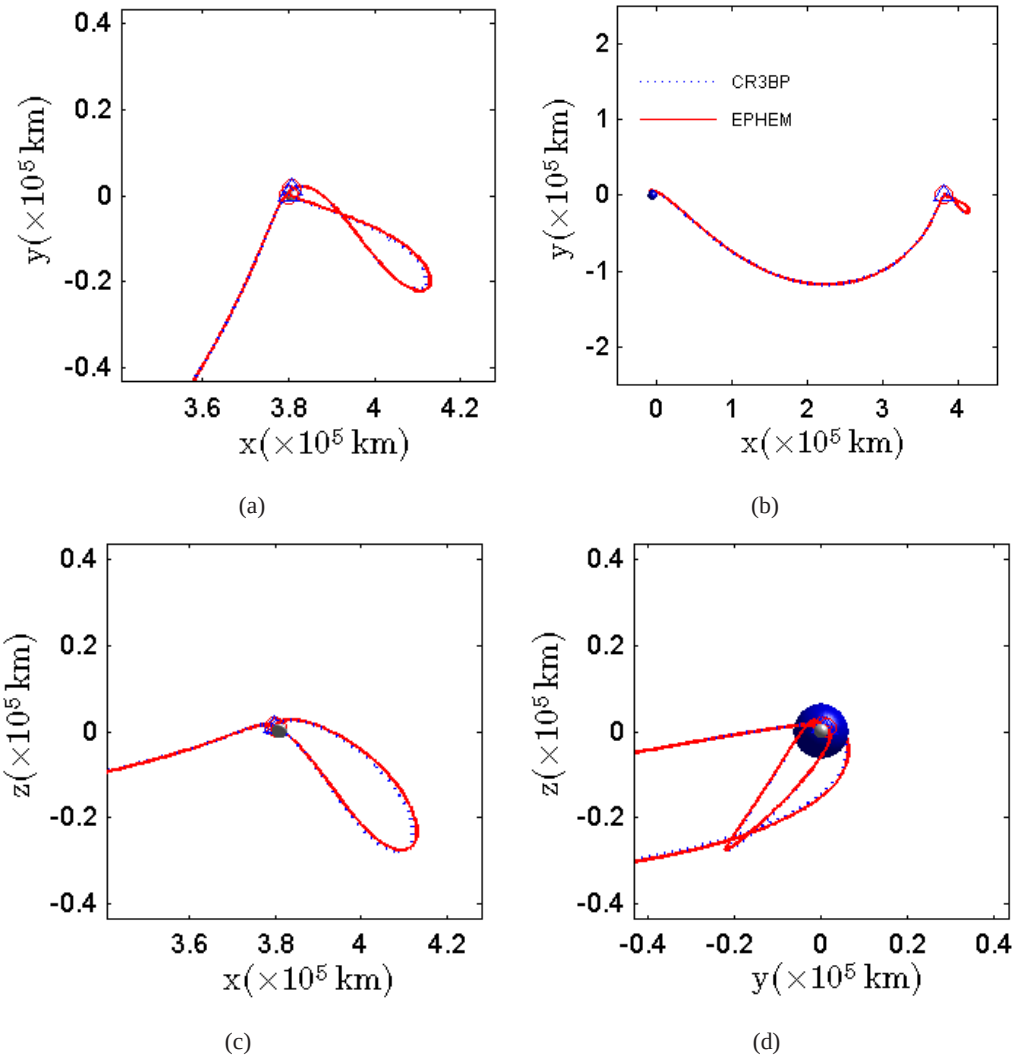

Figure 6. Two-Burn Solution: ΔV = 1 km/sec

Entry Parameter Sensitivities

The numerical evidence collected during the dispersion analysis reveals some useful information regarding the entry constraint coupling and the impact of errors in specific constraints on the targeting process. As previously mentioned, the arrows illustrated in the legend of Figures 3(a)-3(f) indicate the direction of the flow along each dispersion loci. A notable feature present in each and every one of these figures is that the flow evolves in opposite directions for latitude and flight path angle. The sensitivities observed from Figures 3(a)-3(f) and Table 2, along with the flow direction along the loci, suggest a coupling between flight path angle and latitude that may lead to conflicts during the convergence process and, as a result, an increased number of iterations. To explore this further, the present section offers a closer look at entry constraint coupling and its impact on targeter performance.

The next few examples are devoted to characterizing the sensitivity of the targeting process to errors in longitude, latitude, and azimuth when targeting one of these quantities simultaneously along with altitude and flight path angle. The data in Tables 3, 4, and 5 is associated with two different startup arcs; the three impulse 1.0 km/sec solution previously presented, and the two impulse 0.96 km/sec solution. Each of these arcs exhibit the desired altitude and flight path angle that was specifically targeted by the multiple shooting process previously discussed. However, the remaining entry parameters were unconstrained at the time. Thus, once the converged solution is identified, the entry state is characterized by a unique unconstrained latitude, longitude, and azimuth. Using these three solutions as startup arcs, Tables 3, 4, and 5 are compiled in an effort to identify how large the entry error in each of these three parameters can be before the targeting process is significantly affected. In each case, four parameters are always targeted simultaneously; the total cost ($\Delta V < 1.5$ km/sec), the altitude (121.912 km), flight path angle (-5.86 deg) and either (a) the longitude, (b) the latitude, or (c) the azimuth. The number listed in the first column of each table represents the error relative to the unconstrained value. Thus, for Solution 1, associated with an unconstrained longitude of roughly 76°, a -135° error suggests that the target longitude is -59°. Since the startup arc is currently at 76° longitude, the targeting process has to correct a -135° initial error relative to the startup arc.

Of the five entry parameters targeted, the data in Table 3 suggests that converging altitude, flight path angle, and longitude simultaneously is a relatively simple to achieve, in contrast to Latitude, in Table 4, where the size of the error at entry and the quality of the initial guess can significantly affect the convergence process. The flight path azimuth exhibits improved convergence behavior over latitude, but errors are not as easily corrected as those in longitude.

Longitude Sensitivity: Recall that the latitude and flight path angle were previously identified to be the most sensitive parameters according to the Hill sphere dispersion analysis. Furthermore, the flow along the dispersion loci for these two parameters proceeded in opposite directions relative to each other. Thus, it is possible that correcting an error in flight path angle introduces an error in latitude. Then, attempting to correct the resulting error in latitude introduces a greater error in flight path angle. In essence, these two constraints can be at odds with each other during a targeting process, which would explain the large number of unconverged cases in Table 4 over a seemingly minuscule error in latitude. For entry errors in longitude, no convergence threshold is apparent. The results in Table 3 suggest that the targeter[4,5] is able to converge for all cases considered, despite the fact that the entry errors spanned the circumference of the globe. However, some cases do experience larger performance degradation, particularly cases that employed Solution 1 (i.e. the three-burn 1.0 km/sec solution) as inputs. For example, 30 iterations are required to converge the

Solution 1 input with an entry longitude error of 135°, and 14 iterations are required when the entry error is -135°. In contrast, only 7 iterations are required to converge the Solution 2 input with entry error 135°, and 8 iterations for a -135° error. This may easily be attributed to the entry timing and the relative location of the lunar interface state for Solution 1 vs. Solution 2 with respect to the Hill sphere.

Table 3. Example 1: Longitude Sensitivity

Longitude Perturbation	Solution 1 (Unconstr: 76.012189°)		Solution 2 (Unconstr: -138.542302°)	
	Iter.	Total ΔV (km/s)	Iter.	Total ΔV (km/s)
$-135°$	14	1.50	8	1.50
$-90°$	14	1.50	6	1.50
$-45°$	7	1.50	5	1.50
$45°$	8	1.50	5	1.50
$90°$	9	1.50	6	1.50
$135°$	30	1.50	7	1.50
$180°$	14	1.50	9	1.50

A better understanding of the differences in convergence behavior is gained by examining the trajectories more closely. In particular, to assess the impact of the quality of the initial guess on the geometry of the final converged arc. Figures 7(a) through 7(f) illustrate a series of Moon centered close-up views corresponding to the $\pm 135°$ entries in Table 3 for Solution 1. The dashed line denotes the initial guess trajectory, and the final trajectory is represented by the solid line. According to Table 3, the +135 perturbation required 30 iterations to converge while the -135 perturbation only required 14. In this case, it is possible that the initial +135 longitude error does not lead to a trajectory that intersects the Hill sphere at all, or does not intersect it in a favorable location relative to the mutual intersection region of the remaining manifolds. Furthermore, as the number of iterations required to converge on a solution increases, the startup arc undergoes increased reshaping to accommodate the constraints. A visible difference between the x-y projection and the yz projections (looking from the Moon towards the Earth) is notable in Figures7(a) through 7(f). Clearly, if the geometry of the lunar departure segment requires significant changes in order to accommodate the targeted entry parameters, as is the case in Figures 7(a) - 7(c), the performance of the algorithm degrades. Thus, it is important that the initial departure arc selected intersect the correct neighborhood of the Hill sphere, one that intersects with the appropriate dispersion loci more closely.

Latitude Sensitivity: In sharp contrast to the longitude results, the performance of the algorithm exhibits increased sensitivity to errors in latitude. The convergence threshold for latitude errors is less than 2°. Results for latitude perturbations at entry, shown in Table 4, indicate that even minor errors can have a negative impact on the efficiency of the targeting process. Using Solution 1 (i.e. the three burn 1.0 km/sec solution) as a startup arc, only half the cases considered converged. As with the longitude results, further insight is gained upon examination of the lunar segments of selected converged trajectories. Figures 8(a) through 8(c) illustrate closeup views of the initial and final trajectories for the Solution 2 input with an entry latitude error of -1.0°. Figures 8(d) - 8(f) and Figures 8(g) - 8(i) show the trajectories for the same input with errors of -0.5° and +0.5°, respectively. Again, the dashed lines represent the initial guess trajectories and the solid lines are the final trajectories. The figures show a strong correlation between convergence and the geometrical disparities of the arcs (initial vs. converged) near the Moon. This is consistent with the trend

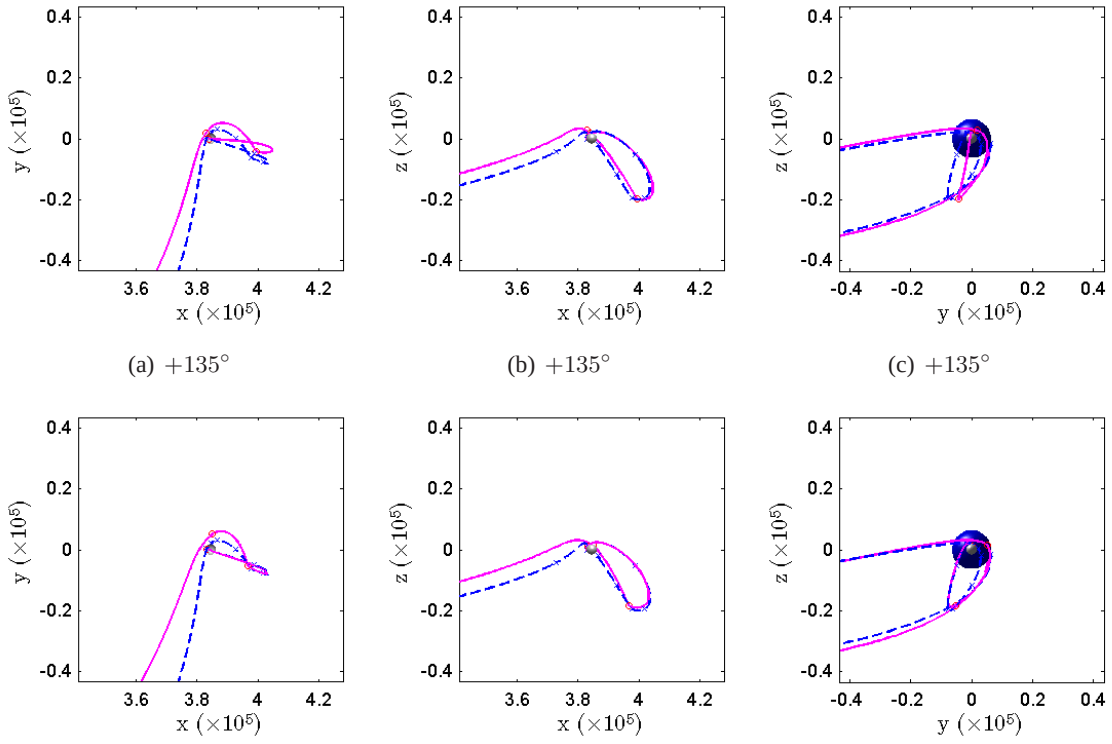

(a) $+135^\circ$ (b) $+135^\circ$ (c) $+135^\circ$

(d) -135° (e) -135° (f) -135°

Figure 7. Solution 1: Impact of Longitude Error on Lunar Departure Geometry

observed for the longitude example; however, for the latitude case, the Hill sphere dispersions reveal that large trajectory changes near the Moon are required to accommodate small changes at entry interface. Thus, latitude is a dynamically sensitive quantity to target and requires significant changes to the departure arc at the Moon. Thus, wider dispersions at the Moon, for small errors at entry, in any parameter, will likely require large adjustments to the departure geometry at the Moon.

Table 4. Example 2: Latitude Sensitivity

Latitude Pert.	Solution 1 (Unconstr: 3.594905°)		Solution 2 (Unconstr: -1.906029°)	
	Iter.	Total ΔV (km/s)	Iter.	Total ΔV (km/s)
$-1.5°$	-	DNC	-	DNC
$-1.0°$	-	DNC	37	1.50
$-0.5°$	9	1.50	11	1.50
$-0.25°$	5	1.44	7	1.50
$0.25°$	5	1.50	5	1.50
$0.5°$	-	DNC	8	1.50
$1.0°$	-	DNC	30	1.50
$1.5°$	20	1.50	-	DNC

DNC = Did Not Converge

Flight Path Azimuth Sensitivity: The results of the flight path azimuth sensitivity analysis are given in Table 5. The flight path azimuth locus on the Hill sphere was narrower than the rest, indicating that small changes in the departure geometry at the Moon are required to accommodate changes in flight path azimuth at entry. That is, as long as the other quantities targeted are not in conflict. In each of the cases presented here, and in the previous sections, the altitude and flight path angle are always targeted as well. Thus, if the flight path azimuth targeted is in conflict with the flight path angle specified, that too will degrade the performance of the targeting algorithm. Although the azimuth results presented here show noticeably improved convergence over the latitude sensitivity results, the convergence threshold for this case is still only $\pm 36°$. The Hill sphere analysis did reveal that the azimuth dispersions exhibit a certain degree of inertia. That is, small changes at Earth entry don't seem to have as significant an impact at the Hill sphere as other parameters do. However, it is also true that the azimuth and flight path angle loci flow in directions that are almost normal to each other. Thus, once the solution sought leaves the vicinity of the intersection of these two loci, it may place the targeter in a neighborhood of phase space that does not include the desired solutions. Thus, the targeting process has to work harder and longer to escape that neighborhood in search for one that offers more auspicious transfers.

To verify this observations, consider the Moon centered close-up views presented here. Figure 9 shows the initial and final Solution 2 trajectories near the Moon for azimuth errors of -24°, in Figures 9(a) - 9(c). Similar images are presented for the +24° error in Figures 9(d) - 9(f). The $-24°$ case requires a total of 38 iterations to converge, while the $+24°$ case converges in only 7. In both cases, the lunar departure geometry is not significantly affected. What is affected, however, is the arrival geometry, best visualized from the yz-plane projections. Curiously, the case that required the least number of iterations to converge is the one that exhibits the most significant changes in arrival geometry. While this may seem counter-intuitive at first, it is actually not surprising. The fact that the overall geometry of the $-24°$ case did not change significantly in 38 iterations suggests a great degree of resistance to small changes. Since the targeting algorithm entails a linear corrections process, one that employs a minimum norm solution, the corrections implemented are the smallest

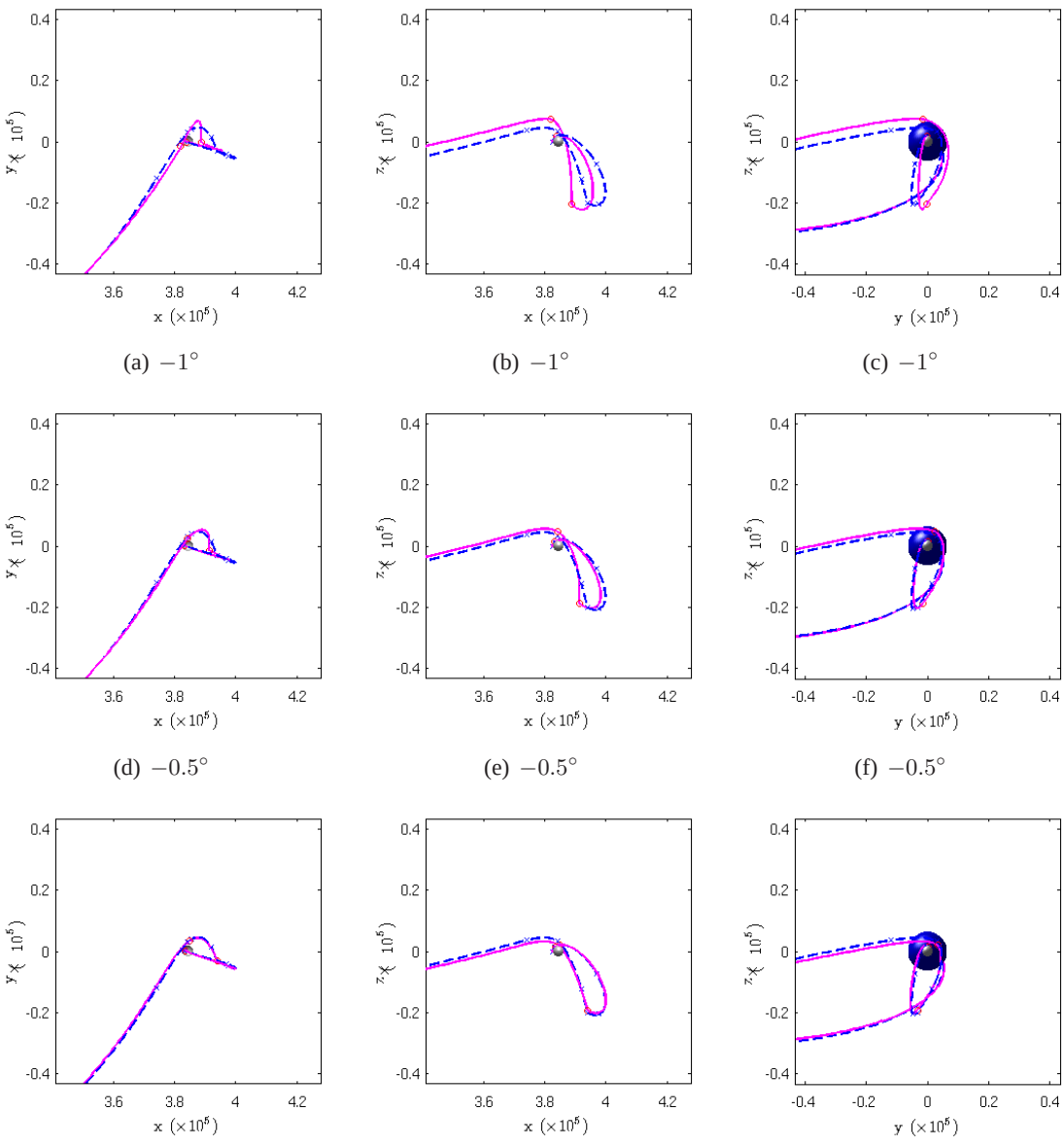

(a) -1° (b) -1° (c) -1°

(d) -0.5° (e) -0.5° (f) -0.5°

(g) $+0.5^\circ$ (h) $+0.5^\circ$ (i) $+0.5^\circ$

Figure 8. Solution 2: Impact of Latitude Error on Lunar Departure Geometry

Table 5. Azimuth Sensitivity

Azimuth Pert.	Solution 1 (Unconstr: 8.985265°)		Solution 2 (Unconstr: 4.172730°)	
	Iter.	Total ΔV (km/s)	Iter.	Total ΔV (km/s)
$-36°$	30	1.50	44	1.50
$-24°$	35	1.50	38	1.50
$-12°$	-	DNC	28	1.50
$-6°$	5	1.16	27	1.50
$6°$	5	1.36	5	1.50
$12°$	11	1.50	6	1.50
$24°$	-	DNC	7	1.50
$36°$	-	DNC	12	1.50

DNC = Did Not Converge

possible change that lead to a feasible solution. The behavior exhibited by this particular solution can be explained in the context of relative stability.

Consider, for instance, the L_1 collinear libration point vs. the L_5 collinear point. The collinear points are all unstable.[17] Thus, small perturbations are promptly amplified as time flows forward. In contrast, the equilateral point L_5 is marginally stable, at least in the linear system. In the ephemeris model, these points do not actually exist. However, the region near the instantaneous libration points exhibit a similar degree of relative stability. Perturbations near the collinear points are quickly amplified, while perturbations near the triangular point grow at a slower rate. It is not surprising, then, to find that there are regions of phase space where solutions are less susceptible to perturbations than others. It is possible that this particular combination of constraints and azimuth perturbations happened to place the solution in a region of phase space that exhibits some level of inertia to small changes.

It was previously noted that the EEI-2 dispersion manifolds extended beyond and around L_5 before intersecting the Hill sphere. Furthermore, the manifolds for EEI-5 and EEI-6 passed interior but very close to L_5 as well. Upon close inspection, a trend is quickly observed. For the entry parameters selected, the azimuth loci on the Hill sphere is narrower in length, and closer to the zero-latitude plane, than any other loci for the cases when the manifolds extended close to L_5 (EEI-2, EEI-5, and EEI-6). Although almost all the dispersion manifolds for EEI-2, EEI-5, and EEI-6 passed near or around L_5, only the azimuth – which affects the Earth arrival plane – was significantly affected by this. The flight path angle loci, for instance, spans a very large latitude range on the Hill sphere for all EEI states considered. The key, it seems, is in the fact that both flight path angle and azimuth are targeted at the same time. One constraint, namely flight path angle, is very sensitive to small changes while the other is not. Thus, the targeting algorithm is susceptible to the inertia induced by the azimuth constraint, in this case. Convergence ensues, but at a much slower rate as a result.

Conclusions

The present study considers the dynamical aspects of the precision entry problem in the Sun-perturbed Earth-Moon system. Earth entry interface state dispersion manifolds are generated and their intersections with the Hill sphere are identified in the synodic frame of the primaries. The spread of the dispersions on the Hill sphere is used to develop an understanding of entry constraint

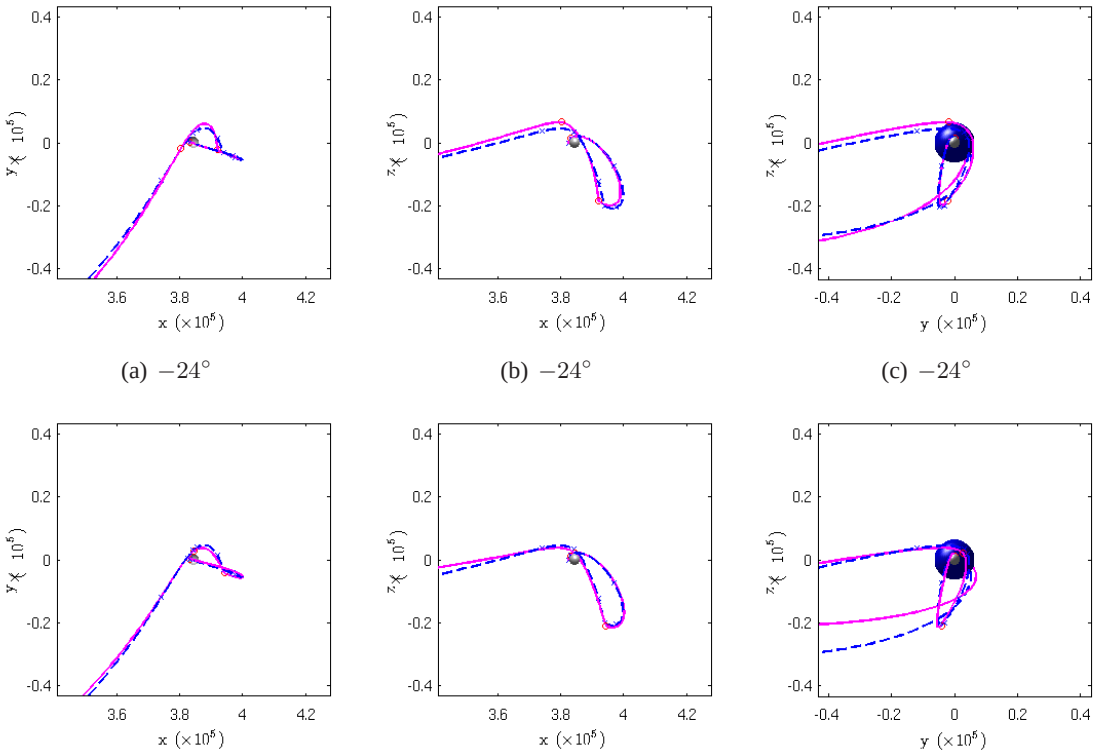

(a) -24° (b) -24° (c) -24°

(d) $+24^\circ$ (e) $+24^\circ$ (f) $+24^\circ$

Figure 9. Solution 2: Impact of Azimuth Error on Lunar Departure Geometry

coupling during a targeting process. The examples presented further demonstrate how third body effects may be harnessed to reduce the overall cost of global precision entry opportunities. A measurable degree of coupling is identified between flight path angle and both azimuth and latitude, though each of a different kind. When targeting multiple entry constraints it is observed that the azimuth constraint introduces a measurable degree of inertia to small perturbations, while the latitude constraint contributes an increased sensitivity to small errors.

ACKNOWLEDGEMENTS

Any opinions, findings, and conclusions or recommendations expressed in this material are those of the authors and do not necessarily reflect the views of the National Aeronautics and Space Administration. This research was a collaborative effort between Purdue University and The University of Texas at Austin. The work was partially supported by NASA under Award Number NNX07AR46G.

REFERENCES

[1] C. A. Ocampo and R. R. Saudemont, "Initial Trajectory Model for a Multi-Maneuver Moon to Earth Abort Sequence," *AAS/AIAA Space Flight Mechanics Meeting*, Feb. 2009. Paper No. AAS 09-195.

[2] D. P. Hamilton and J. A. Burns, "Orbital Stability Zones about Asteroids," *Icarus*, Vol. 92, July 1991, pp. 118–131.

[3] D. P. Hamilton and J. A. Burns, "Orbital stability zones about asteroids : II. The destabilizing effects of eccentric orbits and of solar radiation," *Icarus*, Vol. 96, March 1992, pp. 43–64.

[4] B. G. Marchand, K. C. Howell, and R. S. Wilson, "Improved Corrections Process for Constrained Trajectory Design in the n-Body Problem," *Journal of Spacecraft and Rockets*, Vol. 44, No. 4, 2007, pp. 884–897.

[5] B. G. Marchand, M. W. Weeks, C. W. Smith, and S. K. Scarritt, "Onboard Autonomous Targeting for the Trans-Earth Phase of Orion," *Journal of Guidance, Control, and Dynamics*, 2009. In Press. Also available as AIAA Paper No. 2008-7262.

[6] S. K. Scarritt, B. G. Marchand, and M. W. Weeks, "An Autonomous Onboard Targeting Algorithm Using Finite Thrust Maneuvers," *AIAA Guidance, Navigation, and Control Conference and Exhibit*, Chicago, IL, Aug. 2009. AIAA 2009-6104.

[7] A. E. Bryson and Y.-C. Ho, *Applied Optimal Control: Optimization, Estimation, and Control*. New York: Taylor & Francis, 1975.

[8] D. G. Hull, *Optimal Control Theory for Applications*. New York: Springer-Verlag, 2003.

[9] J. T. Betts, "Survey of Numerical Methods for Trajectory Optimization," *Journal of Guidance, Control, and Dynamics*, Vol. 21, Mar-Apr 1998, pp. 193–207.

[10] J. Betts, *Practical Methods for Optimal Control Using Nonlinear Quadratic Programming*. Philadelphia, PA: Society of Industrial and Applied Mathematics, 2001.

[11] J. Betts and S. Erb, "Optimal Low Thrust Trajectories to the Moon," *SIAM Journal on Applied Dynamical Systems*, Vol. 2, May 2003, pp. 144–170.

[12] J. Betts, "Very Low Thrust Trajectory Optimization Using a Direct SQP Method," *Journal of Computational and Applied Mathematics*, Vol. 120, Aug 2000, pp. 27–40.

[13] M. Lo *et al.*, "GENESIS Mission Design," *Journal of the Astronautical Sciences*, Vol. 49, January-March 2001, pp. 169–184.

[14] B. T. Barden and K. C. Howell, "Fundamental motions near collinear libration points and their transitions," *The Journal of the Astronautical Sciences*, Vol. 46, No. 4, 1998, pp. 361–378.

[15] D. Grebow, M. Ozimek, K. Howell, and D. Folta, "Multi-Body Orbit Architectures for Lunar South Pole Coverage," *Journal of Spacecraft and Rockets*, Vol. 45, March-April 2008, pp. 344–358.

[16] E. Standish, "JPL Planetary and Lunar Ephemerides, DE405/LE405," tech. rep., The Jet Propulsion Laboratory. IOM 312.F98048.

[17] *Theory of Orbits: the Restricted Problem of Three Bodies*. New York: Academic Press, 1967.

[18] *Numerical Solution of Two Point Boundary Value Problems*, Vol. 24 of *CBMS-NSF Regional Conference Series in Applied Mathematics*. Society for Industrial Mathematics, 1976.

[19] G. Gómez, J. Masdemont, and C. Simó, "Quasihalo Orbits Associated with Libration Points," *The Journal of the Astronautical Sciences*, Vol. 46, No. 2, 1998, pp. 135–176.